processes

MDPI

Article

Structured Thin Films Based on Synergistic Effects of $MnTa_2O_6$ Oxide and *bis*-Carboxy-phenyl-substituted Porphyrins, Capable to Inhibit Steel Corrosion

Mihaela Birdeanu [1], Camelia Epuran [2], Ion Fratilescu [2] and Eugenia Fagadar-Cosma [2,*]

[1] National Institute for Research and Development in Electrochemistry and Condensed Matter, Plautius Andronescu Street 1, 300224 Timisoara, Romania; mihaelabirdeanu@gmail.com
[2] Institute of Chemistry "Coriolan Dragulescu", Mihai Viteazu Ave. 24, 300223 Timisoara, Romania; ecamelia@acad-icht.tm.edu.ro (C.E.); ionfratilescu@acad-icht.tm.edu.ro (I.F.)
* Correspondence: efagadar@yahoo.com or efagadarcosma@acad-icht.tm.edu.ro

Abstract: Covering steel surfaces with suitable materials with the capacity to protect against corrosion represents a challenge for both research and industry, as steel, due to its paramount utility, is the most recycled material. This study presents the realization of new sandwich type materials based on 5,10-(4-carboxy-phenyl)-15,20-(4-phenoxy-phenyl)-porphyrin or 5,15-(4-carboxy-phenyl)-10,20-diphenylporphyrin and $MnTa_2O_6$ designed to improve corrosion inhibition of steel in aggressive media. The thin films, designed as single- or sandwich-type structures were obtained on carbon steel through the drop-casting technique. Morphological investigations of thin films were carried out by field emission-scanning electron microscopy (SEM) and atomic force microscopy (AFM). The inhibition of a steel corrosion process was evaluated in an aggressive environment of 0.1 M HCl by performing electrochemical investigations such as open circuit potential (OCP) and the potentiodynamic polarization technique. The influence of variations in the cathodic Tafel slopes β_c and anodic Tafel slopes β_a over the corrosion rates was discussed. The best corrosion inhibition efficiency of 91.76% was realized by the steel electrode covered with sandwich-type layers of 5,15-(4-carboxy-phenyl)-10,20-diphenylporphyrin on the bottom layer and $MnTa_2O_6$ on the top. The effect of location of the COOH groups in the *cis* or *trans* position on the tetrapyrrolic ring was also discussed to understand the corrosion inhibition mechanism.

Keywords: porphyrins; oxide; corrosion inhibition; SEM; AFM; potentiodynamic polarization technique; Tafel representation

Citation: Birdeanu, M.; Epuran, C.; Fratilescu, I.; Fagadar-Cosma, E. Structured Thin Films Based on Synergistic Effects of $MnTa_2O_6$ Oxide and *bis*-Carboxy-phenyl-substituted Porphyrins, Capable to Inhibit Steel Corrosion. *Processes* **2021**, *9*, 1890. https://doi.org/10.3390/pr9111890

Academic Editors: Yanbo Pan, Zhenmeng Peng, Chunhai Yi and Xiaochen Shen

Received: 27 September 2021
Accepted: 18 October 2021
Published: 22 October 2021

1. Introduction

Carbon steel and its alloy derivatives play a vital role in many domains of engineering, such as constructions, all kinds of machinery, petroleum refineries equipment, and pipes due to their excellent resistance, and both physical and mechanical properties [1,2]. One of the main drawbacks of using equipment made of carbon steel is its chemical resistance in an acid environment [3–10]. Steel corrosion inhibitors bring significant benefits when used in descaling or in oil-well-acidizing treatments and in cleaning procedures using acids [11–18]. Among commercially available acids, the most frequently used is hydrochloric acid. Carbon steel and its alloys react very easily in acidic environments, producing large economic losses [19]. The application of the corrosion inhibitors [8–12] leads to a significant reduction in the corrosion of steel in an aggressive acid medium, increasing the feasibility and lifetime of the equipment and installations. Several organic and inorganic compounds deposited as protective layers on metallic surfaces have the desired effect of decreasing the corrosion rate [20,21]. The adsorption of inhibitors on metallic surfaces to uniformly create covering and adherent layers depends on certain physical–chemical properties of the inhibitor, as follows: electronic structure of the whole molecule, nature of grafted functional groups and the capacity to self-aggregate and generate supramolecular architectures [22,23].

Regarding their mechanism for inhibiting corrosion [24], the inorganic inhibitors usually act as anodic or passivation inhibitors or by diminishing the cathodic reaction of the steel by restricting oxygen diffusion. Besides these two mechanisms, the organic inhibitors act also through surface adsorption, thus providing a shield against the steel corrosion [25]. Flat compounds that contain nitrogen atoms, as porphyrins do, can block the corrosion sites with extensive π-bonds [26].

A large number of organic and inorganic materials were tested to evaluate their capacity as corrosion inhibitors. All these studies reveal that organic materials, especially the highly versatile porphyrins and inorganic materials based on pseudo-binary oxides ($ZnTa_2O_6$, $ZnNb_2O_6$, $MgTa_2O_6$, $MgNb_2O_6$), showed significant inhibition efficiency [15,27–31].

The main aim of the present study is to test the steel corrosion inhibition provided by thin layers of two different A_2B_2 porphyrins, containing two COOH-functional groups, namely: 5,10-(4-carboxy-phenyl)-15,20-(4-phenoxy-phenyl)-porphyrin or 5,15-(4-carboxy-phenyl)-10,20-diphenylporphyrin(structures in Figure 1 a and b)in association with $MnTa_2O_6$ pseudo-binary oxide. In order to achieve a high impact, an acid environment of 0.1 M HCl was chosen to perform the corrosion tests. The inhibiting single or sandwich type layers were obtained by drop-casting technique on electrodes of carbon steel.

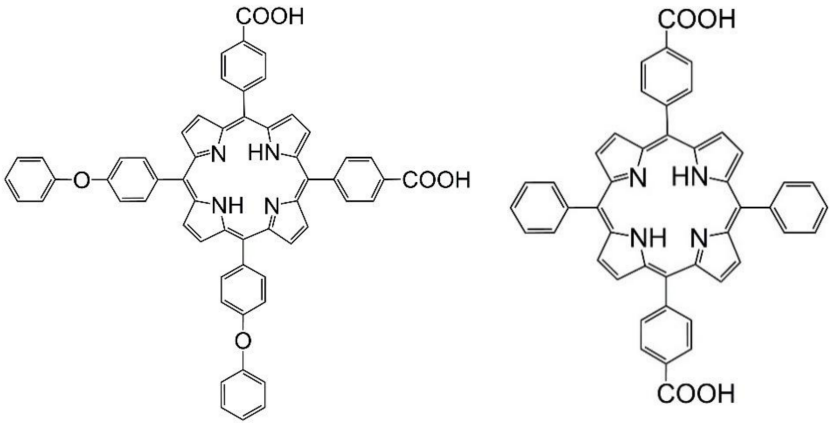

(**a**) (**b**)

Figure 1. Structures of (**a**) 5,10-(4-carboxy-phenyl)-15,20-(4-phenoxy-phenyl)–porphyrin; (**b**) 5,15-(4-carboxy-phenyl)-10,20-diphenylporphyrin.

2. Materials and Methods

2.1. Obtaining of bis-Carboxy-phenyl Substituted Porphyrins

Bis-carboxy-phenyl substituted porphyrins, namely: *cis* 5,10-(4-carboxy-phenyl)-15,20-(4-phenoxy-phenyl)-porphyrin and *trans* 5,15-(4-carboxy-phenyl)-10,20-phenyl-porphyrin, were synthesized by combinatorial Adler–Longo reactions by using two different substituted aldehydes and pyrrole in each condensation reaction, as previously reported [32–34]. In each synthesis, the mixture of the six porphyrin products was separated by optimized HPLC on a Silicagel Preparative Nuleosil 100SI 10 μm 25 × 1.0, reverse-phase column chromatography, using, for the first case, a mixture of three solvents: ethyl acetate (99%, Merck, Darmstadt, Germany): DMSO (98%, Sigma-Aldrich, St. Louis, MO, USA): propionic acid = 96:3:1 (%Vol) (96%, Merck, Darmstadt, Germany). The retention time for *cis* 5,10-(4-carboxy-phenyl)-15,20-(4-phenoxy-phenyl)-porphyrin was 3.613 min. In the case of 5,15-(4-carboxy-phenyl)-10,20-phenyl-porphyrin the retention time was 3.093 min, by using a preparative Kromasil column 100 Sil 25 × 0.4 μm and another mixture of eluents: acetone (99%, Merck, Darmstadt, Germany): toluene = 50:50 (%Vol) (92%, Sigma-Aldrich, St. Louis, MO, USA), at a rate of 1 mL/min.

2.2. Obtaining of $MnTa_2O_6$

$MnTa_2O_6$ was obtained by solid-state synthesis. The precursors used to obtain $MnTa_2O_6$ were tantalum (V) oxide—Ta_2O_5 (99.99%, Merck, Darmstadt, Germany) and manganese nitrate tetrahydrate—$Mn(NO_3)_2 \times 4H_2O$ (99.99%, Sigma-Aldrich, St. Louis, MO, USA) while keeping the molar ratio 1:1. The oxide and the salt were milled and heated in calcination furnace SNOL (Telecomed, Iasi, Romania) at 1100 °C for 3 h with a heating and cooling rate of 5 °C/min.

2.3. Design of Structured Thin Film

All initial materials, 5,10-(4-carboxy-phenyl)-15,20-(4-phenoxy-phenyl)-porphyrin or 5,15-(4-carboxy-phenyl)-10,20-diphenylporphyrin and $MnTa_2O_6$ and $MnTa_2O_6$ pseudo-binary oxide were deposited in single and sandwich layers by drop-casting method on steel (OL) disks, with a diameter of 10 mm and a thickness of 2 mm. The compounds that were deposited in different deposition orders on the steel electrodes (EPI SISTEM, Brasov, Romania) are presented in Table 1.

Table 1. Drop-casting thin film depositions.

Electrode	The Order of the Deposited Materials on Electrodes	Deposition Mode
a	$MnTa_2O_6$	Monolayer
b	5,10-(4-carboxy-phenyl)-15,20-(phenoxy-phenyl)-porphyrin	Monolayer
c	5,15-(4-carboxy-phenyl)-10,20-bis-phenylporphyrin	Monolayer
d	$MnTa_2O_6$/5,10-(4-carboxy-phenyl)-15,20-(phenoxy-phenyl)-porphyrin	Sandwich
e	5,10-(4-carboxy-phenyl)-15,20-(phenoxy-phenyl)-porphyrin/$MnTa_2O_6$	Sandwich
f	$MnTa_2O_6$/5,15-(4-carboxy-phenyl)-10,20-bis-phenylporphyrin	Sandwich
g	5,15-(4-carboxy-phenyl)-10,20-bis-phenylporphyrin/$MnTa_2O_6$	Sandwich

The chemical composition on OL (Mechel Campia Turzii, Romania, low content carbon steel) is (wt. %): Fe = 98, Al = 0.0309, Cu = 0.311, Si = 0.339, Mn = 0.219, Cr = 0.18, Co = 0.0138, C = 0.165, Ni = 0.179, Mo = 0.0339, Pb = 0.05, Nb = 0.0023, Ti = 0.005, Zr = 0.005, V = 0.005, W = 0.05, P = 0.005 and S = 0.005. Before each thin film's deposition, the surfaces of (Ols) were finely polished with emery paper (NIKKEN, Tokyo, Japan) to obtain a mirror-like surface, rinsed with double-distilled water and degreased with ethanol (99.6%, Merck, Darmstadt, Germany).

2.4. Method for Electrode Preparations

The electrochemical investigations of the capacity of the realized thin films to protect against corrosion were performed on a Voltalab Model PGZ 402 potentiostat, equipped with an electrochemical cell, made of a working electrode (consisting in bare (OL) for control or drop-casted modified steel disks), a counter-electrode of platinum wire (Metrohm Analytics Romania SRL, Bucharest/Romania) and a saturated calomel reference electrode (SCE) (Metrohm Analytics Romania SRL, Bucharest/Romania). All potentials were referenced to the standard hydrogen electrode (SHE) (Metrohm Analytics Romania SRL, Bucharest/Romania). The potentiodynamic polarization measurements were recorded at 23 °C ± 1 °C, by sweeping the potential in the - 1.3 V ÷ - 0.6 V domains at a scan rate of 1 mV/s. The corrosive environment was a solution 0.1 M HCl (0.1 N, Merck, Darmstadt, Germany). The open circuit potential (OCP) of the protected electrodes was monitored around 30 min before polarization. The electrodes were fixed into a Teflon (SC NEAGOE FLUOROPOLIMERI SRL, Brasov, Romania) body to obtain a precise active surface of 0.28 cm^2. The measured parameters, such as corrosion potential (E_{corr}), corrosion current density (i_{corr}), polarization resistance (R_p), corrosion rate (ν_{corr}), the anodic (β_a) and the ca-

thodic Tafel slope (β_c), were calculated using VoltaMaster 4 v. 7.09 software. The inhibition efficiency (IE%) was calculated based on the previously reported equation [35].

2.5. Apparatus

The morphologic characteristics of the single- and sandwich-deposited layers were analyzed by field emission-scanning electron microscopy—(SEM)/EDAX (Model INSPECT S) (FEI Company, Hillsboro, OH, USA) with two types of signal-detecting backscattered electrons and secondary electrons (EDS detector), using a low vacuum at a magnification = 100×, high voltage = 25.00 KV and weight distance = 10.6 mm and atomic force microscopy (AFM) apparatus (Nanosurf®EasyScan2, Liestal, Switzerland) using the non-contact mode cantilever (image scan size of 1.1 µm × 1.1 µm, time/line = 1 s, points/line = 1024).

Using the previously reported equations [36] and the Nanosurf®EasyScan 2 soft, the values of average roughness S_a and the mean square root roughness S_q were calculated for each sample. The thickness of the layers (S_y) was also calculated for each deposited layer before and after the corrosion tests. The electrode surface had an area of 1.326 pm^2. Particle size analysis was performed with the AFM software.

A Voltalab Model PGZ 402 potentiostat (Radiometer Analytical—Copenhagen, Denmark) with VoltaMaster 4 software v.7.09 was used for the electrochemical tests.

3. Results and Discussion

2D AFM images of the surfaces for each of the covering layers deposited on OL electrodes, taken before and after corrosion tests, using a non-contact mode cantilever, are presented in Figure 2.

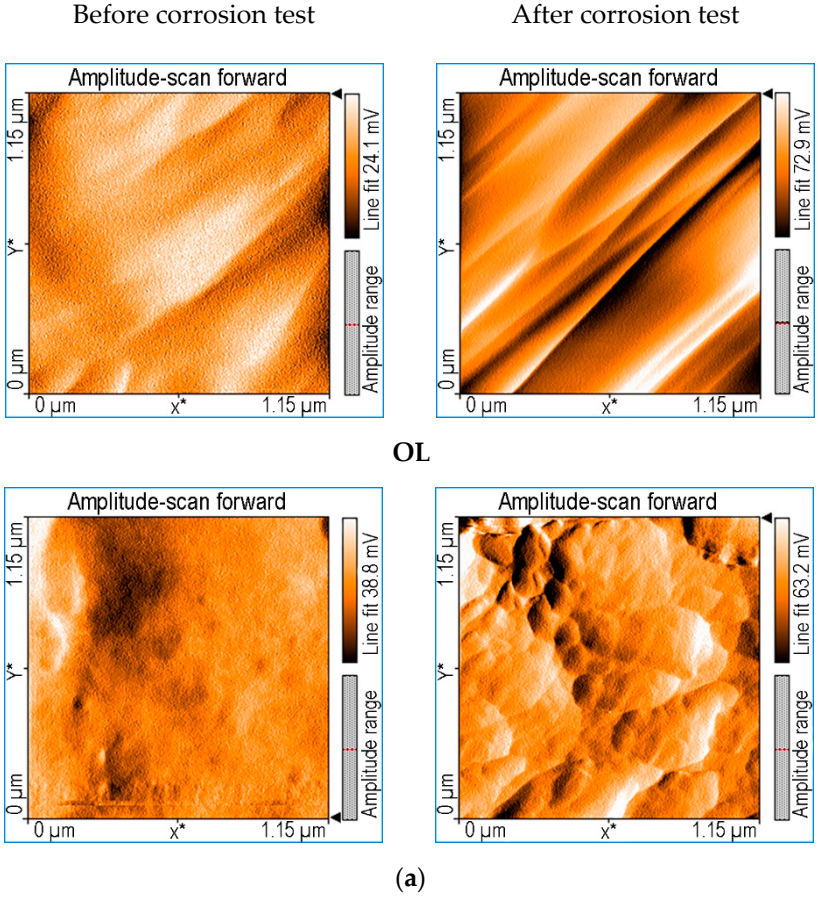

Figure 2. *Cont.*

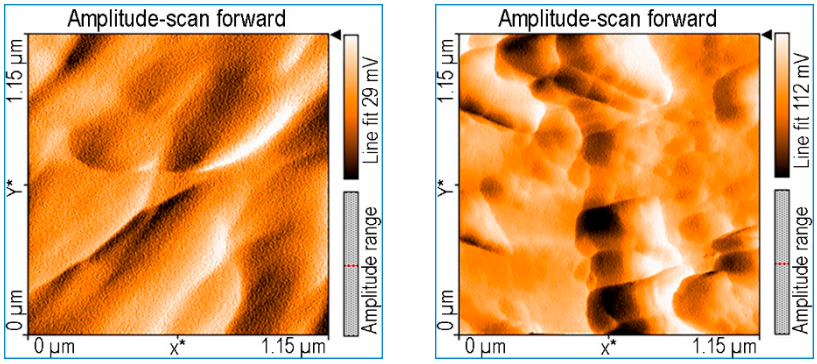

(**b**)

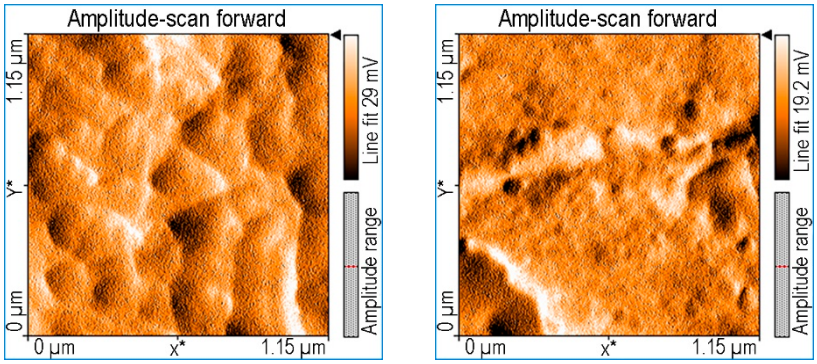

(**c**)

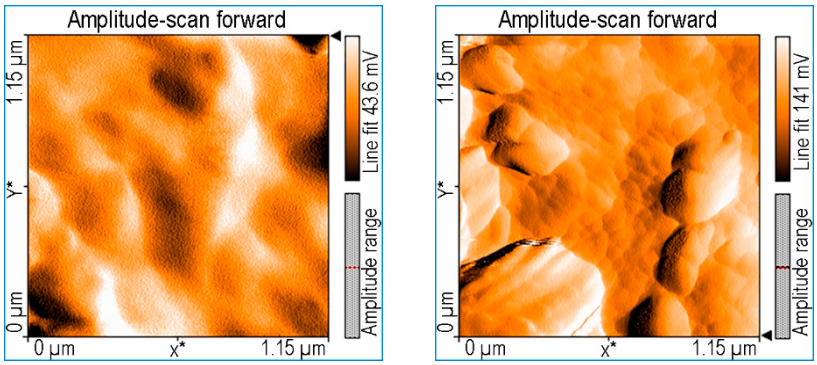

(**d**)

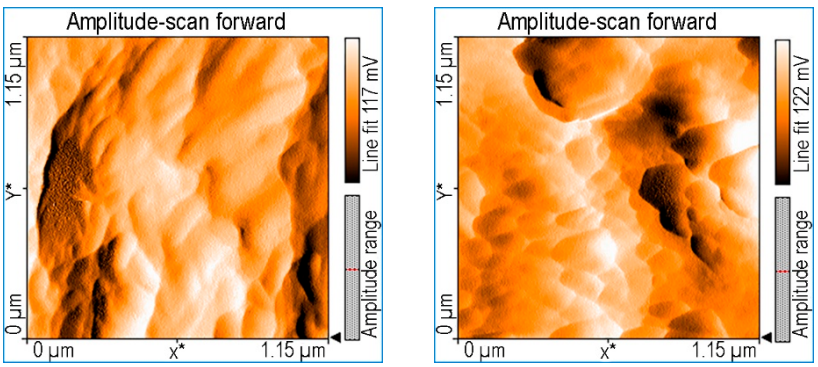

(**e**)

Figure 2. *Cont.*

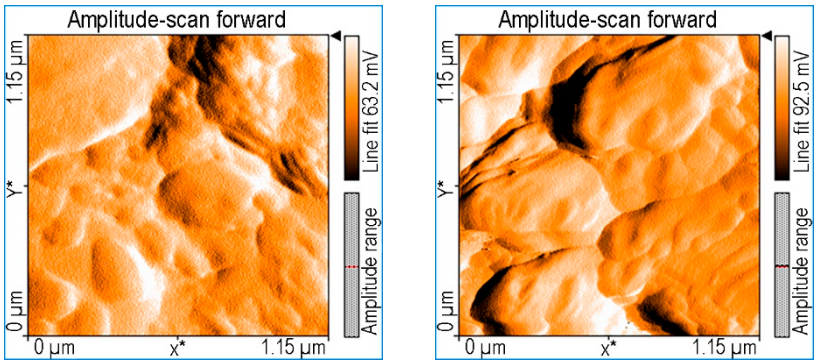

(**f**)

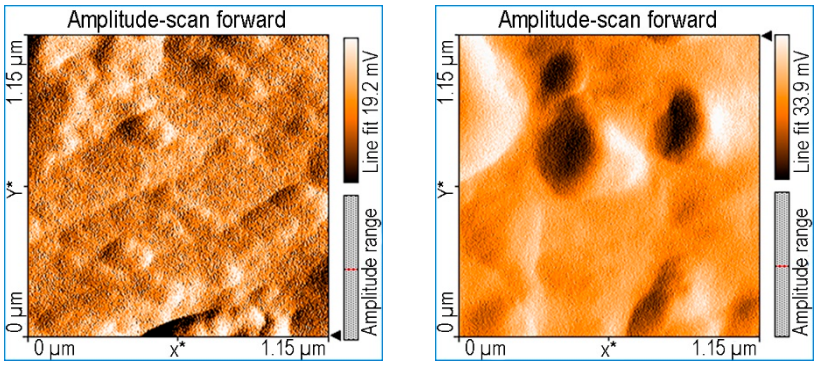

(**g**)

Figure 2. 2D AFM images for the covering layers, before and after corrosion tests: bare OL electrode; (**a**) $MnTa_2O_6$; (**b**) 5,10-(4-carboxy-phenyl)-15,20-(4-phenoxy-phenyl)-porphyrin; (**c**) 5,15-(4-carboxy-phenyl)-10,20-bis-phenylporphyrin; (**d**) $MnTa_2O_6$/5,10-(4-carboxy-phenyl)-15,20-(4-phenoxy-phenyl)-porphyrin; (**e**) 5,10-(4-carboxy-phenyl)-15,20-(4-phenoxy-phenyl)-porphyrin/$MnTa_2O_6$; (**f**) $MnTa_2O_6$/5,15-(4-carboxy-phenyl)-10,20-bis-phenylporphyrin; (**g**) 5,15-(4-carboxy-phenyl)-10,20-bis-phenylporphyrin/$MnTa_2O_6$.

The particle dimensions and nano-roughness of the surfaces are presented in Table 2.

Table 2. Surface particle dimensions and the nano-roughness.

Electrode	Area (pm^2)	S_a before/after (nm)	S_q before/after (nm)	S_y before/after (nm)	Particles Dimension (nm)
OL	1.326	0.3/73.98	2.37/81.52	-	-
a		3.38/60.37	4.02/71.67	22.38/435.73	23
b		4.1/56.99	4.95/63.41	31.40/416.99	28
c		5.65/51.79	7.33/62.53	56.53/384.53	30
d		8.15/48.53	10.40/59.66	66.77/251.42	33
e		11.39/40.52	14.56/56.73	90.61/212.52	35
f		16.19/36.57	20.07/51.73	108.7/193.93	38
g		23.47/33.51	30.69/47.44	165.42/189.8	45

As in Table 2, $MnTa_2O_6$ single layer had the smoothest surface, characterized by the smallest roughness value and, in the case of sandwich layers, higher values were obtained (the highest values are for sandwich layers composed of *trans* 5,15-(4-carboxy-phenyl)-10,20-bis-phenylporphyrin/$MnTa_2O_6$). AFM measurements data provided particle sizes (Table 2) that vary between 23 and 45 nm, with the last value being obtained for the sample with the highest roughness value. As can be observed from Table 2, the differences obtained before and after the corrosion tests for Sa, Sq and Sy are considerably smaller

in the case of steel covered with a sandwich layer consisting of 5,15-(4-carboxy-phenyl)-10,20-bis-phenylporphyrin/$MnTa_2O_6$, meaning that the layer was sufficiently stable in the aggressive medium [37].

Figure 3 shows the most significant morphological aspects of the deposited thin films f and g after performing the corrosion tests. These features (Figure 3a,b) were examined by SEM, and recorded at a magnification of 100×. The sandwich structures present a larger density of particles at the surface. There is a strong relationship between the SEM images aspect and the values for rugosity in the two samples. The non-uniform-type architectures of sample a have a higher value of rugosity [38] than that of sample b, which uniformly displays crystals organized in multiple layers.

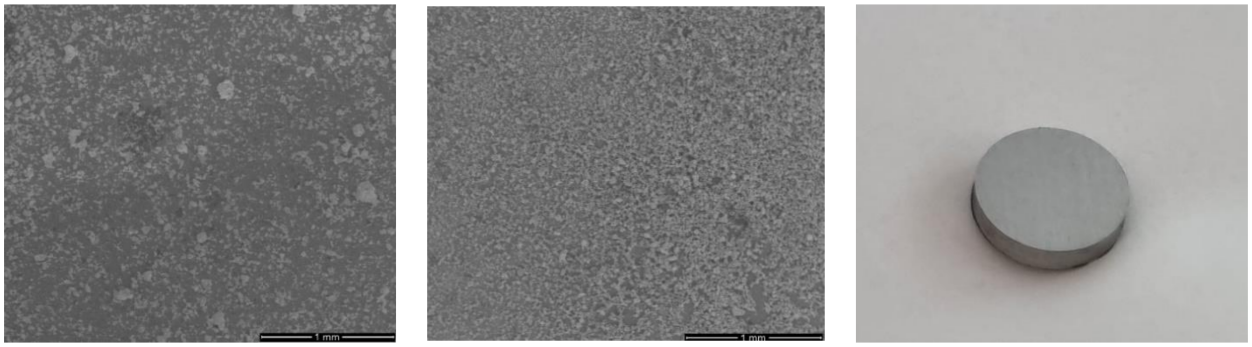

(**a**) (**b**) (**c**)

Figure 3. SEM images for the depositions with the following structures after corrosion tests: (**a**) $MnTa_2O_6$/5,15-(4-carboxy-phenyl)-10,20-bis-phenylporphyrin (optical microscopy); (**b**) 5,15-(4-carboxy-phenyl)-10,20-bis-phenylporphyrin/$MnTa_2O_6$ (optical microscopy); (**c**) is the steel disk electrode (OL), 10 mm diameter and a thickness of 2 mm (macropicture obtained with a Nikon camera, Tokyo, Japan).

The evolution of the OCP versus time measurements (Figure 4) were performed for the bare and modified carbon-steel disk electrodes in 0.1 M HCl solution for 30 min. As can be seen in Figure 4, an initial analysis of these curves shows that, in all cases, including bare electrode, a 30 min exposure time leads to a shift in the free potential toward more negative values. The OCP measurements (Figure 4) showed that the covered electrodes stabilize at around 400–500 s, while the uncoated electrode stabilizes at around 1700 s. This result provides preliminary information on the nature of the processes occurring at the interfaces between metal/thin film and the electrolyte. The OCP is a qualitative indicator of the state of corrosion of the steel substrate in acid medium and helps to determine the immersion time required to reach the steady state [39].

Figure 5 are shows the Tafel plots of the investigated OL electrodes recorded after 30 min OCP in 0.1 M HCl solution. The slopes were determined in the Tafel region of the anodic and cathodic curves before and after reaching the corrosion potential (U). The Tafel parameters, which were calculated using VoltaMaster 4 v. 7.09 software, are presented in Table 3. The degree of inhibition efficiency IE (%) was calculated using the following equation [34].

In Table 3, where the calculated parameters from the Tafel plots are summarized, the corrosion potential (E_{corr}) of the OL electrode is −406.3 mV and the corresponding corrosion current density (i_{corr}) is 0.9548 mA/cm^2. All the thin films deposited in single or sandwich structures on electrodes display significantly lower corrosion current densities in comparison with the OL disk.

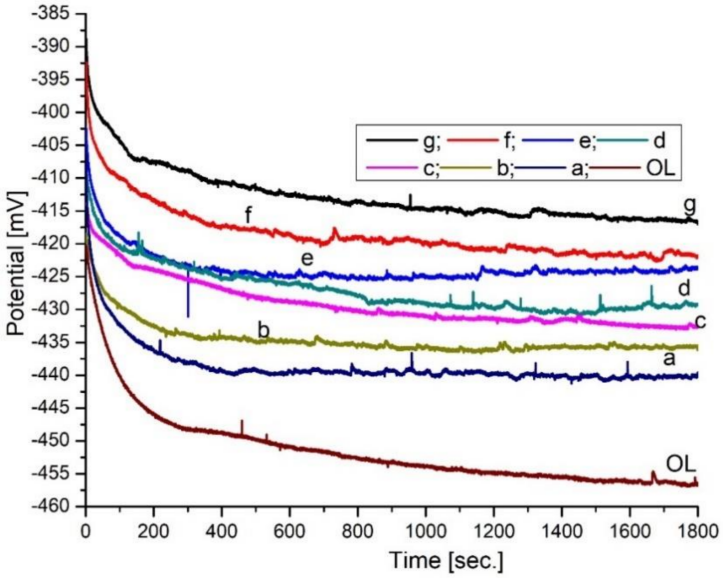

Figure 4. The OCP of the covered electrodes after 30 min immersion in 0.1 M HCl as it follows: OL (bare electrode); (**a**) $MnTa_2O_6$; (**b**) 5,10-(4-carboxy-phenyl)-15,20-(4-phenoxy-phenyl)-porphyrin; (**c**) 5,15-(4-carboxy-phenyl)-10,20-bis-phenylporphyrin; (**d**) $MnTa_2O_6$/5,10-(4-carboxy-phenyl)-15,20-(4-phenoxy-phenyl)-porphyrin; (**e**) 5,10-(4-carboxy-phenyl)-15,20-(4-phenoxy-phenyl)-porphyrin/$MnTa_2O_6$; (**f**) $MnTa_2O_6$/5,15-(4-carboxy-phenyl)-10,20-bis-phenylporphyrin; (**g**) 5,15-(4-carboxy-phenyl)-10,20-bis-phenylporphyrin/$MnTa_2O_6$.

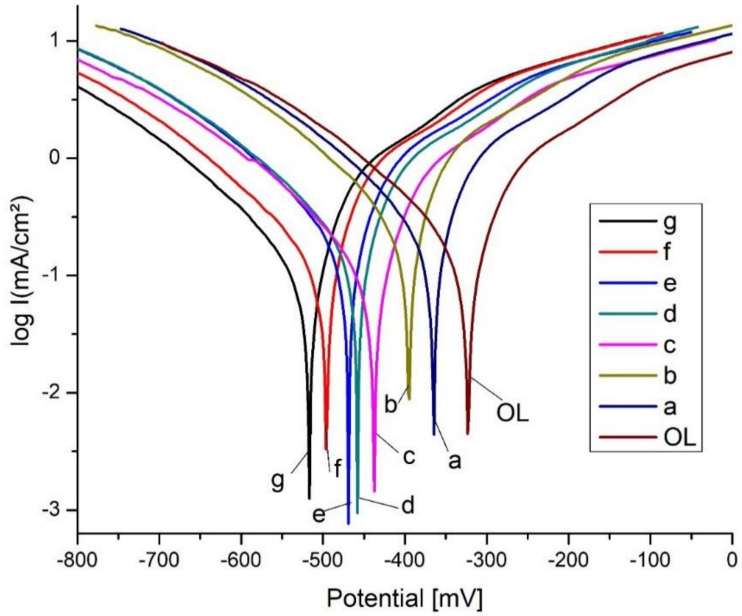

Figure 5. Tafel polarization curves recorded in 0.1 M HCl for the studied electrodes: OL (bare electrode); (**a**) $MnTa_2O_6$; (**b**) 5,10-(4-carboxy-phenyl)-15,20-(4-phenoxy-phenyl)-porphyrin; (**c**) 5,15-(4-carboxy-phenyl)-10,20-bis-phenylporphyrin; (**d**) $MnTa_2O_6$/5,10-(4-carboxy-phenyl)-15,20-(4-phenoxy-phenyl)-porphyrin; (**e**) 5,10-(4-carboxy-phenyl)-15,20-(4-phenoxy-phenyl)-porphyrin/$MnTa_2O_6$; (**f**) $MnTa_2O_6$/5,15-(4-carboxy-phenyl)-10,20-bis-phenylporphyrin; (**g**) 5,15-(4-carboxy-phenyl)-10,20-bis-phenylporphyrin/$MnTa_2O_6$.

Table 3. The Tafel parameters calculated for the protected electrodes immersed in 0.1 M HCl medium for 30 min.

Electrode	E (I = 0) (mV)	R_p ($\Omega \times cm^2$)	i_{corr} (mA/cm^2)	β_a (mV)	β_c (mV)	ν_{corr} (mm/Y)	IE (%)
OL	−406.3	101.35	0.9548	256.9	−423.7	3.256	-
a	−410.3	104.87	0.3781	175.7	−253.7	2.320	60.40
b	−412.9	107.03	0.2690	143.8	−205.1	1.893	71.82
c	−416.9	119.23	0.1602	115.9	−189.3	1.761	83.22
d	−417.2	120.69	0.1349	108.2	−139.6	1.653	85.87
e	−417.7	122.74	0.1289	52.7	−106.2	1.621	86.52
f	−420.3	128.21	0.1028	43.2	−73.5	1.439	89.17
g	−423.5	131.64	0.0790	39.5	−70.7	1.392	91.76

The polarization resistance (R_p) increases from 101.35 $\Omega \times cm^2$, which is characteristic of bare OL, to 131.64 $\Omega \times cm^2$ in the case of 5,15-(4-carboxy-phenyl)-10,20-bisphenylporphyrin/$MnTa_2O_6$. Table 3 presents the recorded Tafel slopes β_a and β_c. The cathodic Tafel slopes β_c are found to increase more significantly than the decreases in the anodic Tafel slopes β_a. The anodic reaction can be presumed to be dependent on activation polarization. Nevertheless, the cathodic reaction cannot be neglected, resulting in further polarization. As β_a is decreasing at a slower rate than the β_c is increasing, the difference in potential between the anodic and cathodic regions is also decreasing and, thus, a lower corrosion rate occurs, as is visible in our case (see Table 3) [36]. The values of the corrosion inhibition efficiencies are influenced by the thickness of the protective layers. The highest inhibition efficiency of 91.76% was found in the case of the OL protected with the 5,15-(4-carboxy-phenyl)-10,20-bisphenylporphyrin/$MnTa_2O_6$ successive layers; this also presented the smallest difference before and after the corrosion tests for Sa, Sq and Sy, meaning that the layer was sufficiently stable in the aggressive medium (see Table 2). This result can also be correlated with SEM image (Figure 3b) that reveals the uniform coverage of the particles over the steel surface.

Analyzing the variation in corrosion potential and corrosion current as the inhibition efficiency is increasing (Table 3), it can be noted, as expected, that the corrosion current is decreasing proportionally to the corrosion rate, and the corrosion potential is shifted to more cathodic values. If a cathodic reaction is involved in the corrosion process, the corrosion potential becomes more negative, as noted in our case. The deposited couple of porphyrin/oxide inhibitors generate a barrier over the metal, thus limiting the contact between the steel and the corrosive acid medium, and finally decreasing the corrosion rate [40].

Another significant but expected result is that the porphyrin 5,15-(4-carboxy-phenyl)-10,20-bisphenylporphyrin, with a smaller steric hindrance and the possibility of creating more continuous supramolecular aggregates, due to the presence in *trans* of two COOH groups, offered the best corrosion protection of the steel surface [31]. Therefore, the *trans*-COOH porphyrin proved to be better suited to our purpose than the porphyrin with the COOH groups in *cis* vicinal position.

The mechanism by which the inhibitors hinder the corrosion of the carbon steel is presumed to be simply based on the physical protection effect caused by the compact and adherent layers of the two bis-carboxyl-substituted porphyrins. These form large supramolecular architectures that are chemically resistant to acids (see Figure 6), thus avoiding direct contact between the acid and the steel [41]. This mechanical barrier effect is because the compact layers of triangular building blocks aggregated both in J and H-type processes is more pronounced in the case of trans-porphyrin (Figure 6a) that in the cis-derivative case (Figure 6b). The cis-porphyrin is helicoidally aggregated in small rings that join together but leave space for little pores and large voids (Figure 6b), which can form places of contact between acid and metal and points at which pitting corrosion begins [42].

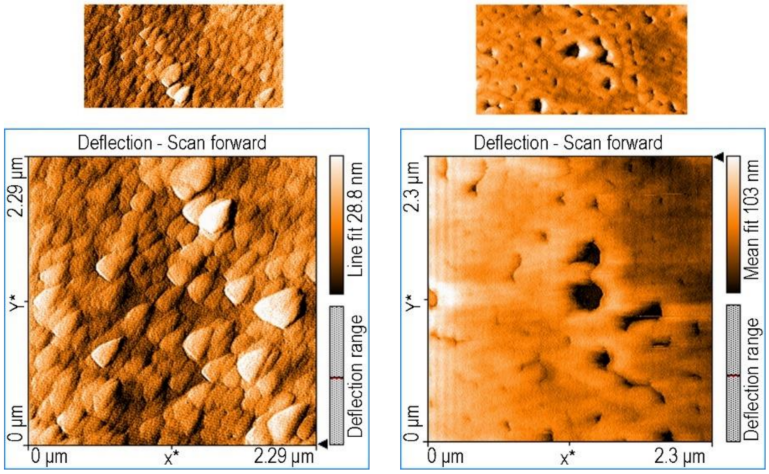

(**a**) (**b**)

Figure 6. AFM images showing better coverage realized by trans 5,15-(4-carboxy-phenyl)-10,20-diphenylporphyrin (**a**) in comparison with *cis* structure, 5,10-(4-carboxy-phenyl)-15,20-(4-phenoxy-phenyl)-porphyrin (**b**).

As can be seen from the SEM images of the cross-sectional sandwich f sample, $MnTa_2O_6$/5,15-(4-carboxy-phenyl)-10,20-bis-phenylporphyrin (Figure 7), there is no cleavage between the steel surface and the covering layers, so it can be expected to have very good mechanical protection against the aggressive HCl medium.

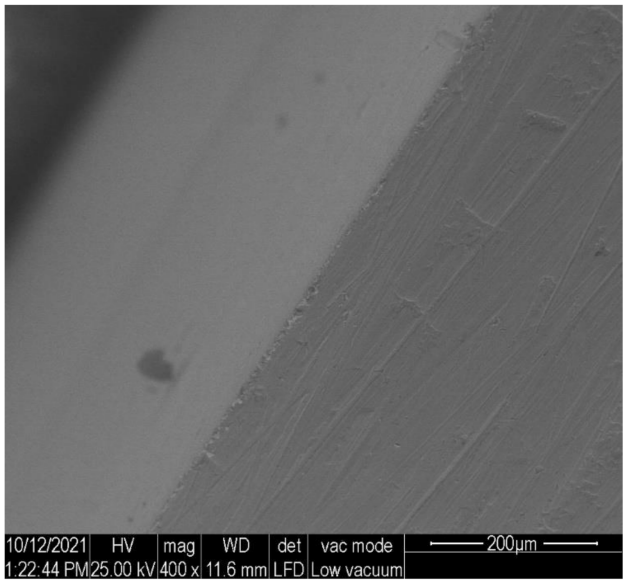

Figure 7. SEM images of the cross-sectional sandwich a sample, $MnTa_2O_6$/5,15-(4-carboxy-phenyl)-10,20-bis-phenylporphyrin.

4. Conclusions

The drop-casting deposition of single and sandwich coatings consisting of $MnTa_2O_6$ pseudo-binary oxide nanomaterials in association with 5,10-(4-carboxy-phenyl)-15,20-(4-phenoxy-phenyl)-porphyrin or 5,15-(4-carboxy-phenyl)-10,20-bis-phenylporphyrin on carbon steel electrodes were realized. The AFM analysis reveals that the main morphological features present in the single layers are preserved in the sandwich layers. Correlating the results obtained from corrosion tests with the features revealed by AFM analysis, it can be concluded that the corrosion inhibition degree increases with the decreasing difference obtained for Sa, Sq and Sy roughness, before and after performing the corrosion

tests. The best value for corrosion inhibition was exhibited by the OL covered with a mixed layer of 5,15-(4-carboxy-phenyl)-10,20-bis-phenylporphyrin and $MnTa_2O_6$ on top, i.e., 91.76% inhibition efficiency. Another significant but expected result is that the porphyrin 5,15-(4-carboxy-phenyl)-10,20-bisphenylporphyrin with a smaller steric hindrance and the possibility to create—due to the presence in *trans* of two COOH groups—more continuous supramolecular aggregates, offered the best corrosion protection on the steel surface. Therefore, the *trans*-COOH porphyrin proved to be better suited to our purpose than the porphyrin with the COOH groups in *cis* vicinal position.

Author Contributions: Conceptualization, M.B. and E.F.-C.; methodology, M.B. and E.F.-C.; software, I.F.; validation, E.F.-C. and M.B.; formal analysis, M.B., C.E and I.F.; investigation, M.B., C.E. and I.F.; resources, M.B. and E.F.-C.; data curation, C.E. and I.F.; writing—original draft preparation, M.B.; writing—review and editing, M.B. and E.F.-C.; visualization, E.F.-C.; supervision, E.F.-C.; project administration, M.B. and E.F.-C.; funding acquisition, E.F.-C. All authors have read and agreed to the published version of the manuscript.

Funding: This research was funded by UEFISCDI, grant number PN III nr. 528PED/2020 "Hybrid ceramics/porphyrins, deposited by pulsed laser deposition as single and sandwich layers for corrosion inhibition of steels in acid environment" and partially by Romanian Academy through Programme 3/2021 from the Institute of Chemistry "Coriolan Dragulescu".

Institutional Review Board Statement: Not applicable.

Informed Consent Statement: Not applicable.

Data Availability Statement: Not applicable.

Conflicts of Interest: All authors declare that the research was conducted in the absence of any commercial or financial relationships that could be construed as a potential conflict of interest.

References

1. Aghili, M.; Yazdi, M.K.; Ranjbar, Z.; Jafari, S.H. Anticorrosion performance of electro-deposited epoxy/amine functionalized graphene oxide nanocomposite coatings. *Corros. Sci.* **2020**, *179*, 109143. [CrossRef]
2. Nikpour, B.; Ramezanzadeh, B.; Bahlakeh, G.; Mahdavian-Ahadi, M. Synthesis of graphene oxide nanosheets functionalized by green corrosion inhibitive compounds to fabricate a protective system. *Corros. Sci.* **2017**, *127*, 240–259. [CrossRef]
3. Khadom, A.A.; Abd, A.N.; Ahmed, N.A. Xanthium strumarium leaves extracts as a friendly corrosion inhibitor of low carbon steel in hydrochloric acid: Kinetics and mathematical studies. *S. Afr. J. Chem. Eng.* **2018**, *25*, 13–21. [CrossRef]
4. Farag, A.; Ismail, A.A.; Migahed, M. Environmental-friendly shrimp waste protein corrosion inhibitor for carbon steel in 1 M HCl solution. *Egypt. J. Pet.* **2018**, *27*, 1187–1194. [CrossRef]
5. Wang, Q.; Tan, B.; Bao, H.; Xie, Y.; Mou, Y.; Li, P.; Chen, D.; Shi, Y.; Li, X.; Yang, W. Evaluation of Ficus tikoua leaves extract as an eco-friendly corrosion inhibitor for carbon steel in HCl media. *Bioelectrochemistry* **2019**, *128*, 49–55. [CrossRef] [PubMed]
6. Miralrio, A.; Vázquez, A.E. Plant Extracts as Green Corrosion Inhibitors for Different Metal Surfaces and Corrosive Media: A Review. *Processes* **2020**, *8*, 942. [CrossRef]
7. Dohare, P.; Chauhana, D.S.; Quraishi, M.A. Expired Podocip drug as potential corrosion inhibitor for carbon steel in acid chloride solution. *Int. J. Corros. Scale Inhib.* **2018**, *7*, 25–37.
8. Fouda, A.S.; Shalabi, K.; E-Hossiany, A. Moxifloxacin Antibiotic as Green Corrosion Inhibitor for Carbon Steel in 1 M HCl. *J. Bio. Tribo. Corros.* **2016**, *2*, 1–13. [CrossRef]
9. Fouda, A.S.; El-Ewady, G.; Ali, A.H. Modazar as promising corrosion inhibitor of carbon steel in hydrochloric acid solution. *Green Chem. Lett. Rev.* **2017**, *10*, 88–100. [CrossRef]
10. Bourazmi, H.; Tabyaoui, M.; EL Hattabi, L.; El Aoufir, Y.; Ebenso, E.E.; Ansari, A. Camphor as an effective corrosion inhibitor for carbon steel in 1M HCl solution: Electrochemical and quantum chemical investigation. *J. Mater. Environ. Sci.* **2018**, *9*, 1058–1074.
11. Bahmani, A.; Arthanari, S.; Shin, K.S. Corrosion behavior of Mg–Mn–Ca alloy: Influences of Al, Sn and Zn. *J. Magnes. Alloys* **2019**, *7*, 38–46. [CrossRef]
12. Alnajjar, M.; Christien, F.; Barnier, V.; Bosch, C.; Wolski, K.; Fortes, A.D.; Telling, M. Influence of microstructure and manganese sulfides on corrosion resistance of selective laser melted 17-4 PH stainless steel in acidic chloride medium. *Corros. Sci.* **2020**, *168*, 108585. [CrossRef]
13. Zhu, H.; Li, X.; Lu, X.; Wang, J.; Hu, Z.; Ma, X. Efficiency of Gemini surfactant containing semi-rigid spacer as microbial corrosion inhibitor for carbon steel in simulated seawater. *Bioelectrochemistry* **2021**, *140*, 107809. [CrossRef] [PubMed]
14. Birdeanu, M.; Vaida, M.; Fagadar-Cosma, E. Hydrothermal synthesis of ZnTa2O6, ZnNb2O6, MgTa2O6 and MgNb2O6 pseudo-binary oxide nanomaterials with anticorrosive properties. *Manuf. Rev.* **2020**, *7*, 39. [CrossRef]

15. Birdeanu, M.; Vaida, M.; Bîrdeanu, A.V.; Fagadar Cosma, E. PLD deposited layers of pseudo-binary zinc oxides and zinc-porphyrin for steel corrosion inhibition. *Corrosion* **2020**, *76*, 734–741. [CrossRef]
16. Vaida, M.; Birdeanu, M.; Bîrdeanu, A.-V. Anticorrosive properties of thin films of pseudo-binary oxide materials deposited by PLD technique on steel. *AIP Conf. Proc.* **2019**, *2071*, 040017–1–040017–6.
17. Birdeanu, M.; Birdeanu, A.V.; Vaida, M.; Orha, C.; Fagadar-Cosma, E. Anticorrosive properties of ZnTa2O6 and ZnV2O6 nanomaterials deposited as sandwich structures by drop casting method in NaCl. In Proceedings of the Nanocon 2017 Conference Proceedings, 9th International Conference of Nanomaterials—Research & Application, Brno, Czech Republic, 18–20 October 2017; pp. 359–365.
18. Birdeanu, M.; Fagadar-Cosma, G.; Sebarchievici, I.; Bîrdeanu, A.V.; Taranu, B.; Taranu, I.; Fagadar-Cosma, E. Zn(Ta1-xNbx)2O6 nanomaterials: Synthesis, characterization and corrosion behaviour. *J. Serb. Chem. Soc.* **2016**, *81*, 163–175. [CrossRef]
19. El-Katori, E.E.; Al Angari, Y.M. Electrochemical and Theoretical Evaluation on the Corrosion Inhibition of Carbon Steel by Organic Selenides in Acidic Medium. *Int. J. Electrochem. Sci.* **2018**, *13*, 4319–4337. [CrossRef]
20. Ahmed, S.K.; Ali, W.B.; Khadom, A.A. Synthesis and investigations of heterocyclic compounds as corrosion inhibitors for mild steel in hydrochloric acid. *Int. J. Ind. Chem.* **2019**, *10*, 159–173. [CrossRef]
21. Yao, S.; Liu, S.; Zeng, G.; Li, X.; Lei, T.; Du, Y. Effect of Manganese on Microstructure and Corrosion Behavior of the Mg-3Al Alloys. *Metals* **2019**, *9*, 460. [CrossRef]
22. Shchukin, D.G.; Zheludkevich, M.; Yasakau, K.; Lamaka, S.; Ferreira, M.; Möhwald, H. Layer-by-Layer Assembled Nanocontainers for Self-Healing Corrosion Protection. *Adv. Mater.* **2006**, *18*, 1672–1678. [CrossRef]
23. Amiri, S.; Rahimi, A. Preparation of supramolecular corrosion-inhibiting nanocontainers for self-protective hybrid nanocomposite coatings. *J. Polym. Res.* **2014**, *21*. [CrossRef]
24. Saha, S.K.; Banerjee, P. A theoretical approach to understand the inhibition mechanismof steel corrosion with two aminobenzonitrile inhibitors. *RSC Adv.* **2015**, *5*, 1120–71130. [CrossRef]
25. Wei, H.; Heidarshenas, B.; Zhou, L.; Hussain, G.; Li, Q.; Ostrikov, K. Green inhibitors for steel corrosion in acidic environment: State of art. *Mater. Today Sustain.* **2020**, *10*, 100044. [CrossRef]
26. Abeng, F.; Ikpi, M.; Ushie, O.; Anadebe, V.; Nyong, B.; Obeten, M.; Okafor, N.; Chukwuike, V.; Nkom, P. Insight into corrosion inhibition mechanism of carbon steel in 2 M HCl electrolyte by eco-friendly based pharmaceutical drugs. *Chem. Data Collect.* **2021**, *34*, 100722. [CrossRef]
27. Birdeanu, M.; Bîrdeanu, A.V.; Vaida, M.; Milovanovic, D.; Lascu, A.; Fagadar-Cosma, E. Corrosion behaviour of ZnTa2O6 pseudo-binary oxide, zinc meso-tetra(4-pyridyl)porphyrin (ZnTPyP) and hybrid ZnTa2O6/ZnTPyP layers deposited by PLD. *Phys. Scr.* **2019**, *94*, 075702. [CrossRef]
28. Vaida, M.; Birdeanu, M.; Lascu, A.; Palade, A.; Fringu, I.; Fagadar-Cosma, E. Anticorrosive coating of steel with hybrid oxide/porphyrine sandwich layers deposited by drop casting method. In Proceedings of the Nanocon 2017 Conference Proceedings, Brno, Czech Republic, 18–20 October 2017; pp. 372–377.
29. Bîrdeanu, A.V.; Birdeanu, M.; Fagadar-Cosma, E. Corrosion protection characteristics of ceramics, porphyrins and hybrid ceramics/porphyrins, deposited as single and sandwich layers, by pulsed laser deposition (PLD). *J. Alloys Compd.* **2017**, *706*, 220–226. [CrossRef]
30. Birdeanu, M.; Birdeanu, A.V.; Popa, I.; Taranu, B.; Peter, F.; Creanga, I.; Palade, A.; Fagadar-Cosma, E. Comparative research regarding corrosion protective effect of different sandwich type nanostructures obtained from porphyrins and pseudo-binary oxides by changing the deposition order. In Proceedings of the NANOCON 2014 Conference Proceedings, Brno, Czech Republic, 5–7 November 2014; TANGER Ltd.: Ostrava, Czech Republic, 2015; pp. 262–268.
31. Fagadar-Cosma, E.; Fagadar-Cosma, G.; Vasile, M.; Enache, C. Synthesis, Spectroscopic and Self-Assembling Characterization of Novel Photoactive Mixed Aryl-Substituted Porphyrin. *Curr. Org. Chem.* **2012**, *16*, 931–941. [CrossRef]
32. Fagadar-Cosma, E.; Vlascici, D.; Birdeanu, M.; Făgădar-Cosma, G. Novel fluorescent pH sensor based on 5-(4-carboxy-phenyl)-10,15,20-tris(phenyl)-porphyrin. *Arab. J. Chem.* **2019**, *12*, 1587–1594. [CrossRef]
33. Vlascici, D.; Făgădar-Cosma, E.; Popa, I.; Chiriac, V.; Gil-Agusti, M. A Novel Sensor for Monitoring of Iron(III) Ions Based on Porphyrins. *Sensors* **2012**, *12*, 8193–8203. [CrossRef]
34. Ahmad, Z. *Principles of Corrosion Engineering and Corrosion Control*; Butterworth-Heinemann/IChemE Series; Elsevier: Amsterdam, The Netherlands, 2006; p. 377.
35. Kapaklis, V.; Poulopoulos, P.; Karoutsos, V.; Manouras, T.; Politis, C. Growth of thin Ag films produced by radio frequency magnetron sputtering. *Thin Solid Films* **2006**, *510*, 138–142. [CrossRef]
36. Ge, J.; Isgor, O. Effects of Tafel slope, exchange current density and electrode potential on the corrosion of steel in concrete. *Mater. Corros.* **2007**, *58*, 573–582. [CrossRef]
37. Burstein, G.T.; Vines, S.P. Repetitive Nucleation of Corrosion Pits on Stainless Steel and the Effects of Surface Roughness. *J. Electrochem. Soc.* **2001**, *148*, B504–B516. [CrossRef]
38. MacLeod, I.D. In-situ Corrosion Measurements of WWII Shipwrecks in Chuuk Lagoon, Quantification of Decay Mechanisms and Rates of Deterioration. *Front. Mar. Sci.* **2016**, *3*. [CrossRef]
39. Wong, P.K.; Kwok, C.T.; Man, H.C.; Cheng, F.T. Laser surface alloying (LSA) of copper for electrical erosion resistance. In *Laser Surface Modification of Alloys for Corrosion and Erosion Resistance*; Elsevier: Amsterdam, The Netherlands, 2012; pp. 288–319.

40. Ameh, P.O.; Eddy, N.O. Theoretical and experimental studies on the corrosion inhibition potentials of 3-nitrobenzoic acid for mild steel in 0.1 M H2SO4. *Cogent Chem.* **2016**, *2*. [CrossRef]
41. Singh, A.; Lin, Y.; Quraishi, M.A.; Olasunkanmi, L.O.; Fayemi, O.E.; Sasikumar, Y.; Ramaganthan, B.; Bahadur, I.; Obot, I.B.; Adekunle, A.S.; et al. Porphyrins as Corrosion Inhibitors for N80 Steel in 3.5% NaCl Solution: Electrochemical, Quantum Chemical, QSAR and Monte Carlo Simulations Studies. *Molecules* **2015**, *20*, 15122–15146. [CrossRef] [PubMed]
42. Zhang, Y.; Yang, C.; Zhao, L.; Zhang, J. Study on the Electrochemical Corrosion Behavior of 304 Stainless Steel in Chloride Ion Solutions. *Int. J. Electrochem. Sci.* **2021**, *16*, 210251. [CrossRef]